Supporting Information

# Influence of Ligand Field on Magnetic Anisotropy in a Family of Pentacoordinate $Co^{II}$ Complexes

*Joydev Acharya,[a] Arup Sarkar,[b] Pawan Kumar,[a] Vierandra Kumar,[a] Jessica Flores Gonzalez,[c] Olivier Cador,[c] Fabrice Pointillart,*[c] Gopalan Rajaraman,*[b] and Vadapalli Chandrasekhar*[a,d]*

[a]Department of Chemistry, Indian Institute of Technology Kanpur, Kanpur-208016, India. E-mail: vc@iitk.ac.in, http://www.iitk.ac.in

[b]Department of Chemistry, Indian Institute of Technology Bombay, Powai,Mumbai-400 076, India. E-mail: rajaraman@chem.iitb.ac.in

[c]Institut des Sciences Chimiques de Rennes, UMR 6226 CNRS-Université deRennes 1,263 Avenue du Général Leclerc, 35042 Rennes Cedex, France. E-mail: fabrice.pointillart@univ-rennes1.fr

[d]Tata Institute of Fundamental Research, 36/P, Gopanpally Village, Serilingampally Mandal, Ranga Reddy District, Hyderabad 500107, India.

**Table S1**. Selected bond lengths (Å) and angels (˚) in complex **1-3**.

| Bond Length (Å) | | | | | | | |
|---|---|---|---|---|---|---|---|
| Complex | Co-N1 | Co-N2 | Co-N3 | Co-X1 (X= Cl/Br) | Co-X2 (X= Cl/Br) | Co-N4 | Co-N5 |
| **1** | 2.069(2) | 2.243(2) | 2.069(2) | 2.289(5) | 2.323(5) | - | - |
| **2** | 2.063(3) | 2.313(3) | 2.079(3) | 2.4384(6) | 2.4948(6) | - | - |
| **3** | 2.038(1) | 2.301(1) | 2.0614(1) | - | - | 1.984(2) | 2.026(2) |

| Bond angle(˚) | | | | | |
|---|---|---|---|---|---|
| Complex **1** | | Complex **2** | | Complex **3** | |
| Cl1—Co1—Cl2 | 100.478(2) | Br1—Co1—Br2 | 106.51(2) | N3—Co1—N2 | 77.34(5) |
| N1—Co1—Cl1 | 136.06(4) | N2—Co1—Br2 | 95.08(7) | N1—Co1—N3 | 115.76(5) |
| N1—Co1—Cl2 | 96.35(4) | N2—Co1—Br1 | 158.35(7) | N1—Co1—N2 | 76.90(5) |
| N1—Co1—N2 | 76.25(6) | N1—Co1—Br2 | 99.96(8) | N4—Co1—N3 | 105.86(6) |
| N2—Co1—Cl1 | 90.14(4) | N1—Co1—Br1 | 100.78(8) | N4—Co1—N1 | 129.89(6) |
| N2—Co1—Cl2 | 169.34(4) | N1—Co1—N2 | 76.56(1) | N4—Co1—N2 | 86.69(5) |
| N3—Co1—Cl1 | 103.45(5) | N1—Co1—N3 | 146.25(1) | N4—Co1—N5 | 100.77(6) |
| N3—Co1—Cl2 | 99.86(5) | N3—Co1—Br2 | 100.01(8) | N5—Co1—N3 | 99.20(6) |
| N3—Co1—N1 | 113.23(6) | N3—Co1—Br1 | 99.25(8) | N5—Co1—N1 | 98.93(6) |
| N3—Co1—N2 | 76.59(6) | N3—Co1—N2 | 74.81(1) | N5—Co1—N2 | 172.44(6) |

**Table S2**. Crystal data and structure refinement parameters of complexes.

| Complex | **1** | **$1_{Zn}$** | **2** | **$2_{Zn}$** | **3** |
|---|---|---|---|---|---|
| Formula | $C_{23}H_{29}Cl_2CoN_3O$ | $C_{22}H_{25}Cl_2ZnN_3$ | $C_{22}H_{25}Br_2CoN_3$ | $C_{22}H_{25}Br_2N_3Zn$ | $C_{24}H_{25}CoN_5S_2$ |
| g/mol | 493.32 | 467.72 | 550.20 | 556.64 | 506.54 |
| Crystal system | monoclinic | triclinic | triclinic | triclinic | triclinic |
| Space group | *P*21/n | *P*-1 | *P*-1 | *P*-1 | *P*-1 |
| *a*/Å | 16.4698(8) | 8.3183(14) | 8.4526(6) | 8.4626(5) | 8.47120(10) |
| *b*/Å | 8.1305(4) | 10.3241(18) | 10.2684(8) | 10.2744(6) | 9.4205(2) |
| *c*/Å | 17.6932(9) | 13.067(2) | 13.3275(11) | 13.2348(7) | 15.8080(2) |
| $\alpha$ (°) | 90 | 98.325(5) | 99.010(2) | 98.374(2) | 101.4480(10) |
| $\beta$ (°) | 100.979(2) | 92.150(5) | 90.814(2) | 90.925(2) | 91.1720(10) |
| $\gamma$(°) | 90 | 110.353(5) | 110.221(2) | 109.403(2) | 102.3220(10) |
| *V*/Å$^3$ | 2325.9(2) | 1036.3(3) | 1069.15(14) | 1071.24(11) | 1205.34(3) |
| *Z* | 4 | 2 | 2 | 2 | 2 |
| $\rho_c$/g cm$^{-3}$ | 1.409 | 1.499 | 1.709 | 1.726 | 1.396 |
| $\mu$/mm$^{-1}$ | 0.987 | 1.456 | 4.553 | 4.889 | 0.907 |
| *F*(000) | 1028.0 | 484.0 | 550.0 | 556.0 | 526.0 |
| Crystal size (mm$^3$) | 0.02 × 0.02 × 0.02 | 0.02 × 0.02 × 0.02 | 0.02 × 0.02 × 0.02 | 0.02 × 0.02 × 0.02 | 0.36 × 0.308 × 0.179 |
| $\theta$ range (deg) | 4.69 to 56.634 | 4.268 to 56.768 | 4.292 to 56.636 | 4.858 to 56.602 | 5.438 to 57.738 |
| Limiting indices | -21 ≤ h ≤ 21, -10 ≤ k ≤ 10, -23 ≤ l ≤ 23 | -11 ≤ h ≤ 11, -13 ≤ k ≤ 13, -17 ≤ l ≤ 17 | -11 ≤ h ≤ 11, -13 ≤ k ≤ 13, -17 ≤ l ≤ 17 | -11 ≤ h ≤ 11, -13 ≤ k ≤ 13, -17 ≤ l ≤ 17 | -11 ≤ h ≤ 11, -12 ≤ k ≤ 11, -14 ≤ l ≤ 21 |
| Reflns collected | 36319 | 15060 | 17222 | 16819 | 20127 |
| Ind reflns | 5773 [$R_{int}$ = 0.0427] | 5151 [$R_{int}$ = 0.0766] | 5251 [$R_{int}$ = 0.0384] | 5317 [$R_{int}$ = 0.0653] | 5549 [$R_{int}$ = 0.0398] |
| Completeness to $\theta$ (%) | 100 | 100 | 98 | 100 | 100 |
| Refinement method | Full-matrix least-squares on $F^2$ | Full-matrix least-squares on $F^2$ | Full-matrix least-squares on $F^2$ | Full-matrix least-squares on $F^2$ | Full-matrix least-squares on $F^2$ |
| Data/restraints/ parameters | 5773/0/287 | 5151/12/250 | 5251/0/256 | 5317/0/256 | 5549/0/303 |
| Goodness-of-fit on $F^2$ | 1.060 | 1.041 | 0.920 | 1.047 | 1.071 |
| Final R indices [$I > 2\theta(I)$] | $R_1$ = 0.0335, $wR_2$ =0.0783 | $R_1$ = 0.0664, $wR_2$ =0.1808 | $R_1$ = 0.0297, $wR_2$ =0.0980 | $R_1$ = 0.0389, $wR_2$ =0.0835 | $R_1$ = 0.0329, $wR_2$ =0.0825 |
| R indices (all data) | $R_1$ = 0.0420, $wR_2$ = 0.0831 | $R_1$ = 0.0789, $wR_2$ = 0.1948 | $R_1$ = 0.0445, $wR_2$ = 0.1249 | $R_1$ = 0.0552, $wR_2$ = 0.0993 | $R_1$ = 0.0381, $wR_2$ = 0.0857 |

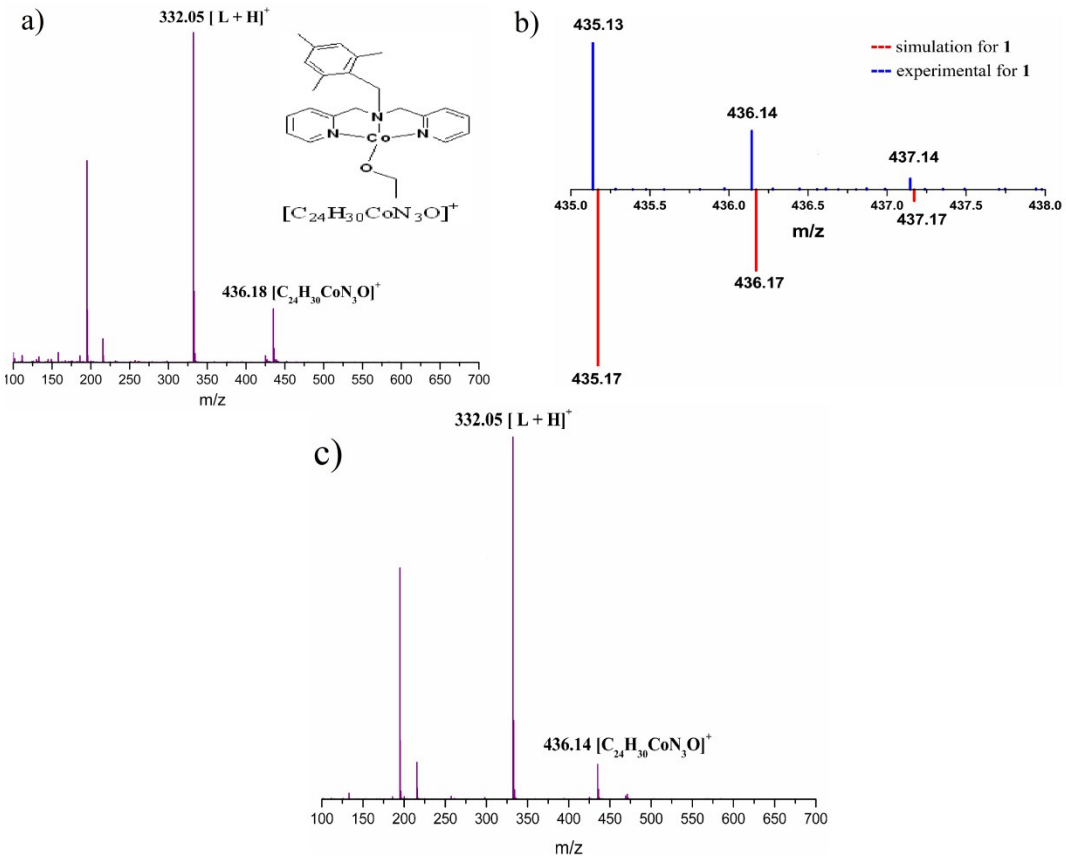


**Figure S1**. a) Full range ESI-MS spectra of **1** and structure of $[C_{24}H_{30}CoN_3O]^+$ (inset), b) isotopic distribution pattern of the species combining experimental and simulation pattern, c) similar full range spectra of **2**.

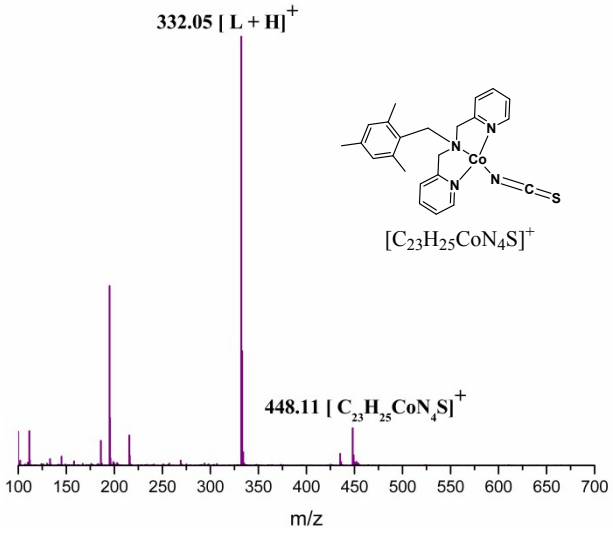


**Figure S2**. a) Full range ESI-MS spectra of **3** and structure of $[C_{22}H_{25}CoN_4S]^+$ (inset).

---

S H A P E  v2.1  Continuous Shape Measures calculation

(c) 2013  Electronic Structure Group, Universitat de Barcelona

Contact:  llunell@ub.edu

| Sl. No. | Geometry | CShM value for **1** | CShM value for **2** | CShM value for **3** |
|---|---|---|---|---|
| 1 | Pentagon($D_{5h}$) | 30.704 | 33.010 | 31.689 |
| 2 | Vacant octahedron($C_{4v}$) | 4.967 | 3.367 | 5.604 |
| 3 | Trigonal bipyramid($D_{3h}$) | **2.371** | 6.452 | **1.238** |
| 4 | Spherical square pyramid($C_{4v}$) | 4.992 | **1.741** | 4.956 |
| 5 | Johnson trigonal bipyramid J12($D_{3h}$) | 3.897 | 7.601 | 2.778 |

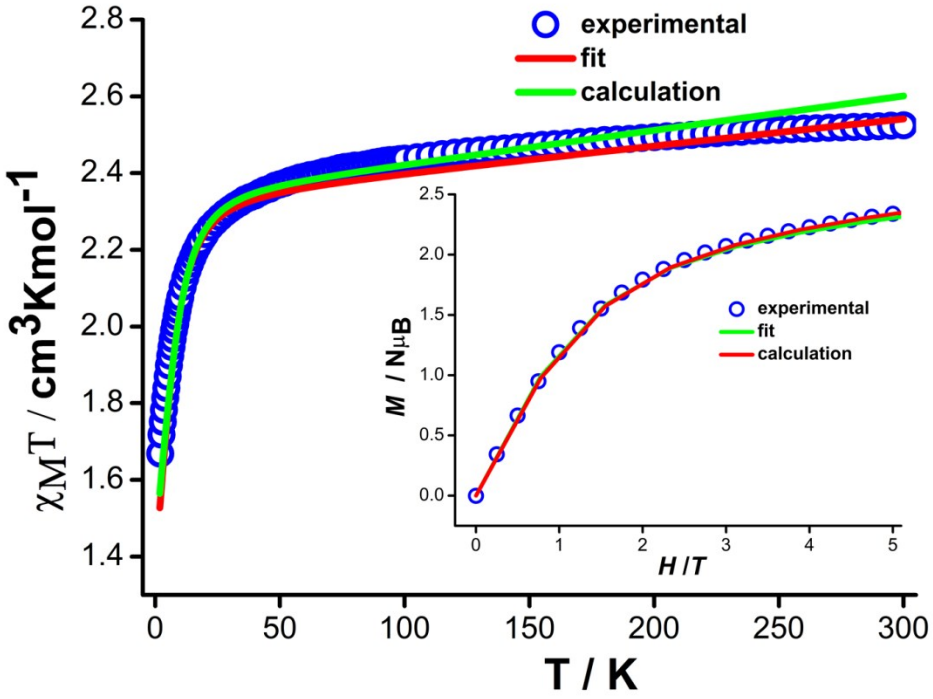


**Figure S3**. Temperature-dependent dc magnetic susceptibility plots of **3**, respectively; (inset) Field-dependent magnetization plots for **3** respectively at 2K. The solid red lines in all the panels represent the best fits obtained after simultaneous fitting of the magnetic data taking negative *D* value of using PHI. The solid green lines in all the panels represent simulations of

the experimental magnetic data considering negative *D* value of the computed SH parameters obtained from CASSCF/NEVPT2 calculation.

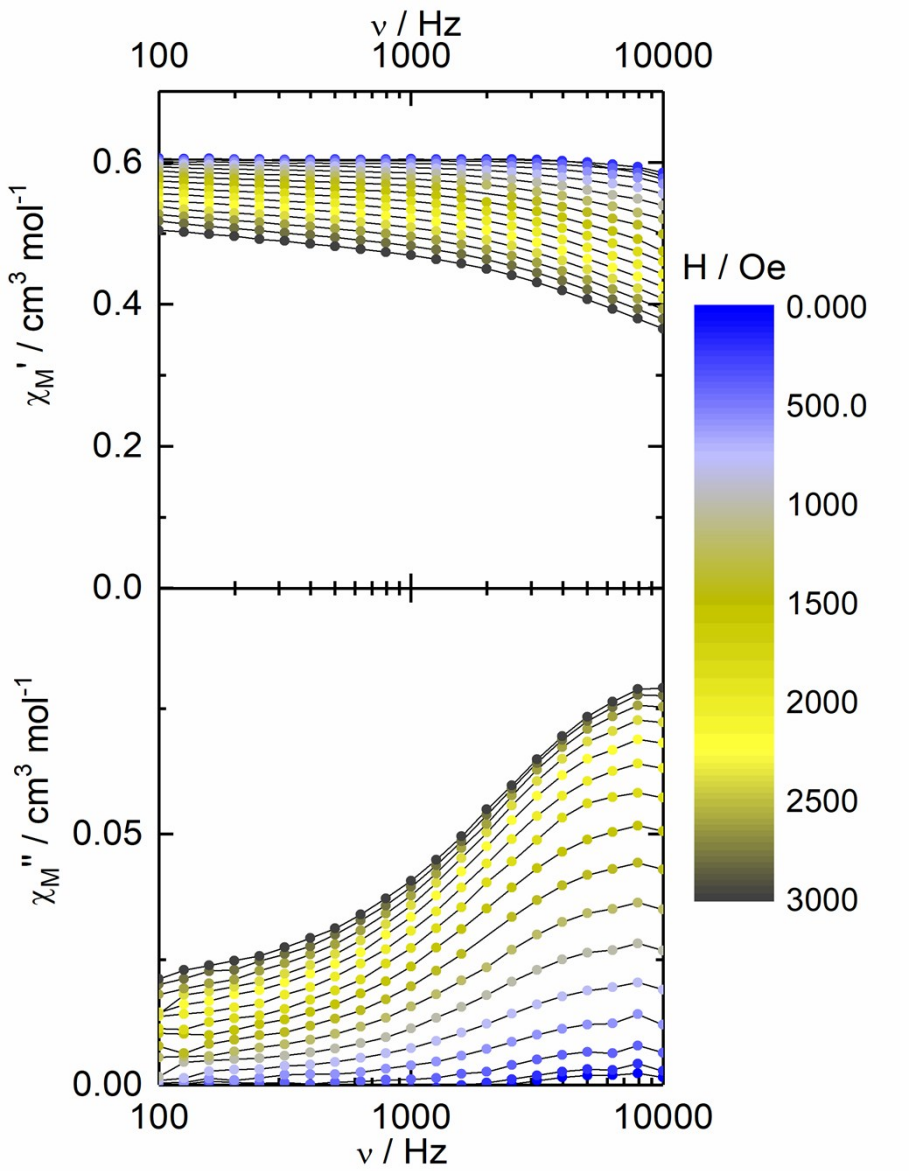


**Figure S4**. Frequency dependences of the in-phase, $\chi_M$', and out-of-phase, $\chi_M$'', components of the AC susceptibility measured at 2 K at various external DC fields for complex **1**.

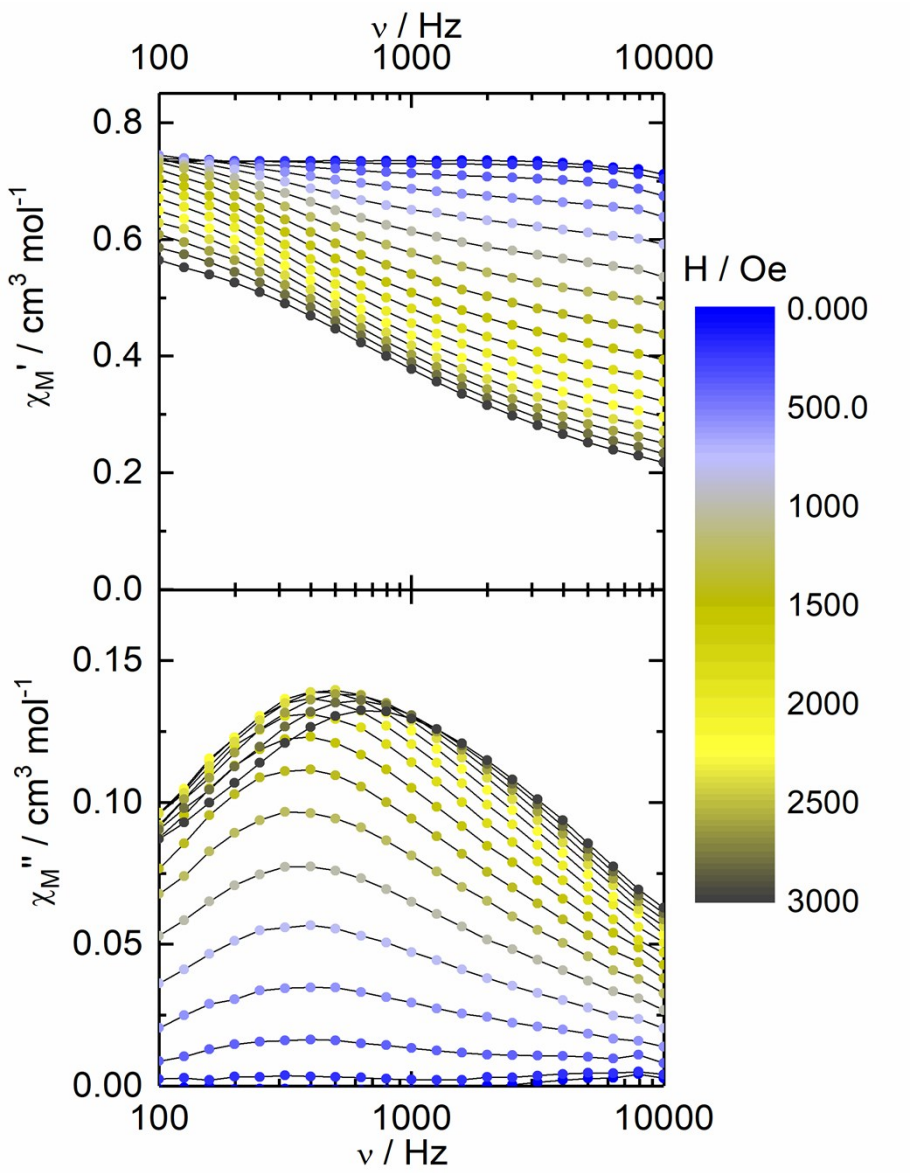


**Figure S5**. Frequency dependences of the in-phase, $\chi_M$', and out-of-phase, $\chi_M$'', components of the AC susceptibility measured at 2 K at various external DC fields for complex **2**.

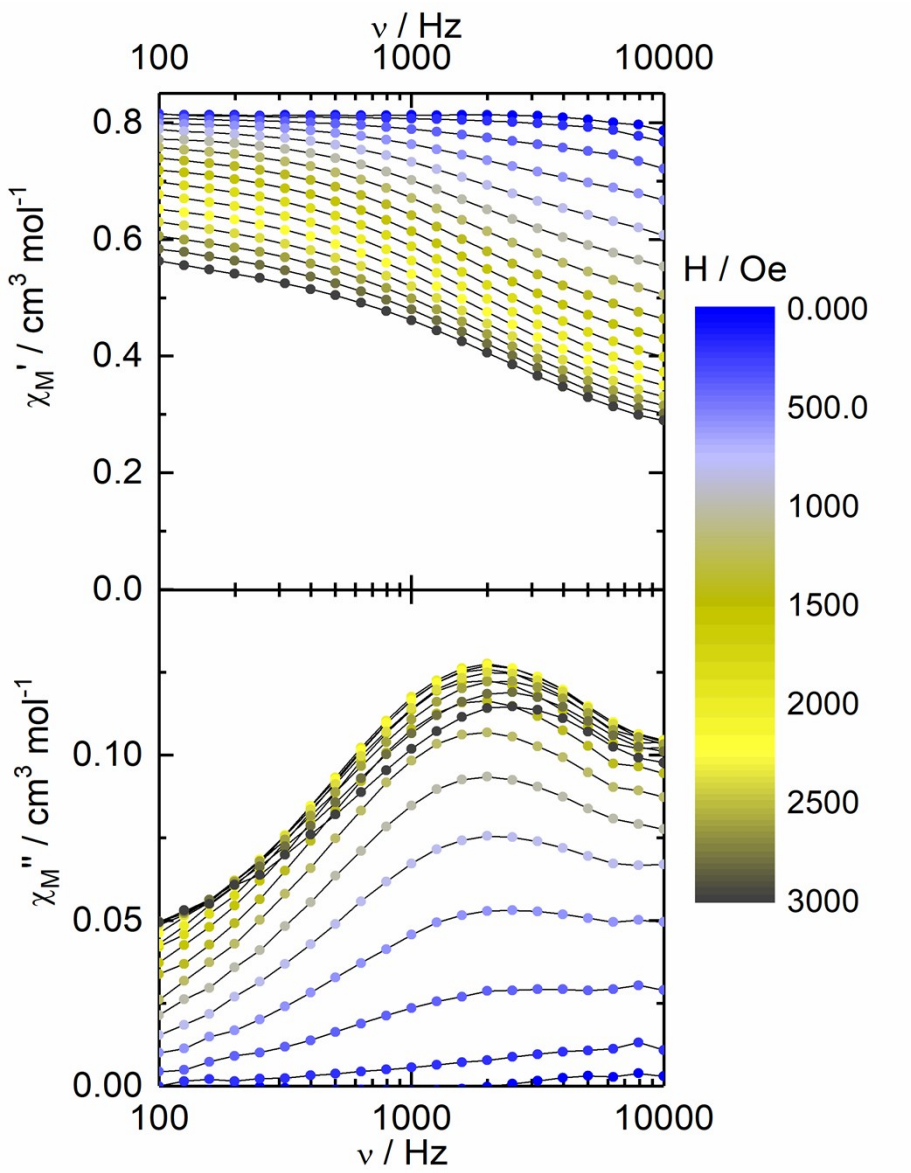


**Figure S6**. Frequency dependences of the in-phase, $\chi_M$', and out-of-phase, $\chi_M$'', components of the AC susceptibility measured at 2 K at various external DC fields for complex **3**.

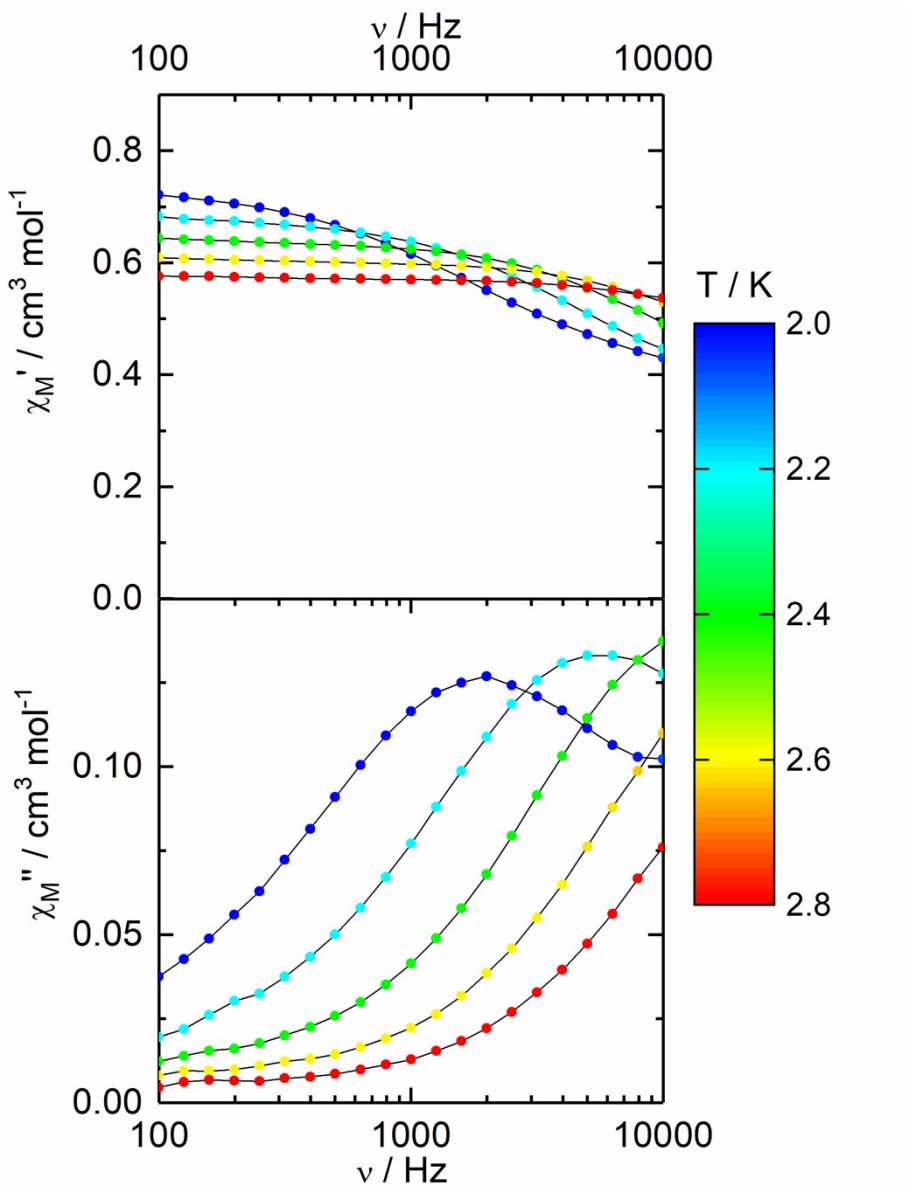


**Figure S7**. Temperature variations of $\chi_M$' and $\chi_M$'' for complex **3** as a function of the frequency,ν, of the oscillating AC field measured at an external DC field of 1600 Oe.

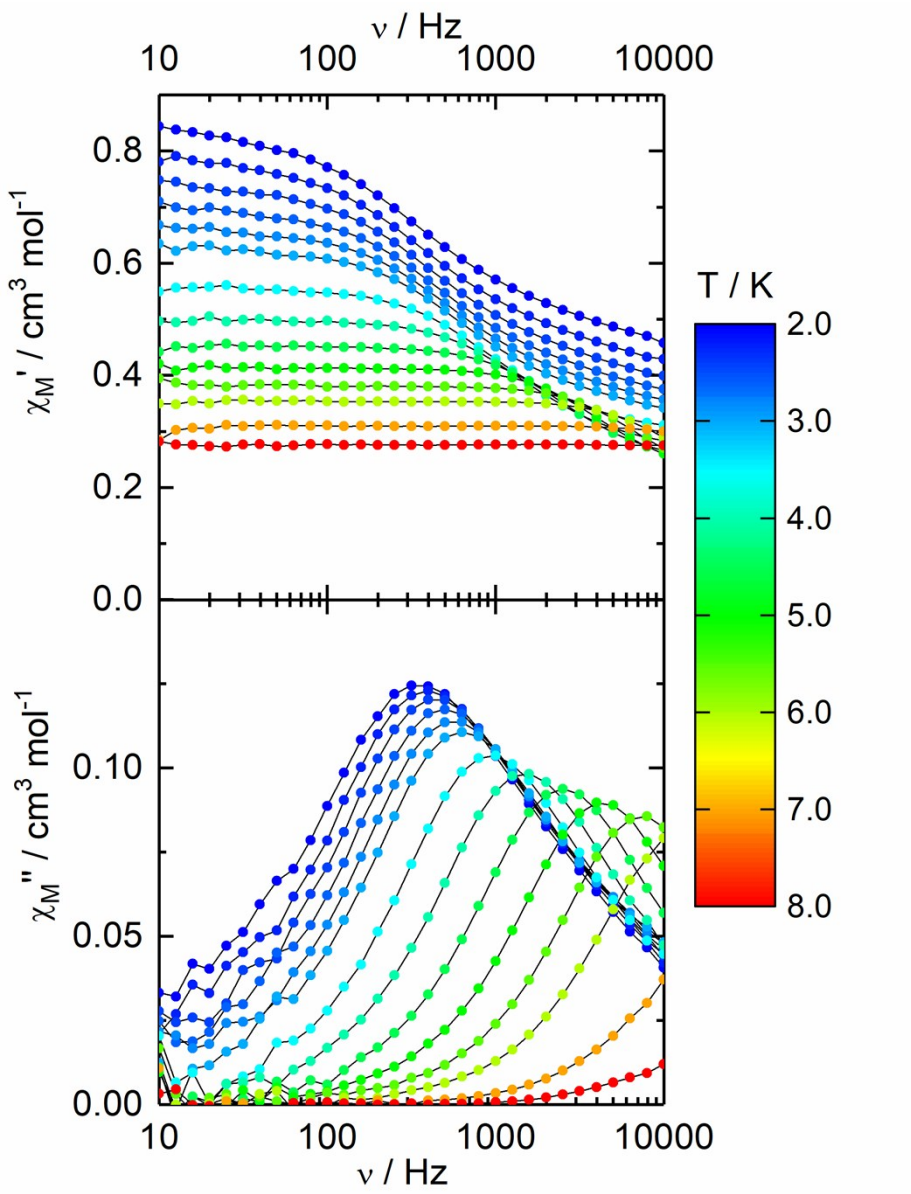


**Figure S8**. Temperature variations of $\chi_M$' and $\chi_M$'' for compound **2** as a function of the frequency, $\nu$ of the oscillating AC field measured at an external DC field of 1400 Oe.

**Extended Debye model**

$$\chi_M' = \chi_S + (\chi_T - \chi_S)\frac{1+(\omega\tau)^{1-\alpha}\sin\left(\alpha\frac{\pi}{2}\right)}{1+2(\omega\tau)^{1-\alpha}\sin\left(\alpha\frac{\pi}{2}\right)+(\omega\tau)^{2-2\alpha}}$$

$$\chi_M'' = (\chi_T - \chi_S)\frac{(\omega\tau)^{1-\alpha}\cos\left(\alpha\frac{\pi}{2}\right)}{1+2(\omega\tau)^{1-\alpha}\sin\left(\alpha\frac{\pi}{2}\right)+(\omega\tau)^{2-2\alpha}}$$

With $\chi_T$ the isothermal susceptibility, $\chi_S$ the adiabatic susceptibility, $\tau$ the relaxation time and $\alpha$ an empiric parameter which describe the distribution of the relaxation time. For SMM with only one relaxing object $\alpha$ is close to zero. The extended Debye model was applied to fit simultaneously the experimental variations of $\chi_M$' and $\chi_M$'' with the frequency $\nu$ of the oscillating field ($\omega = 2\pi\nu$). Typically, only the temperatures for which a maximum on the $\chi_M$'' vs. $\nu$ curves, have been considered (see figure here below for an example). The best fitted parameters $\tau$, α, $\chi_T$, $\chi_S$ are listed in table S3 with the coefficient of determination $R^2$.

**Table S3**. Best fitted parameters ($\chi_T$, $\chi_S$, $\tau$ and $\alpha$) with the extended Debye model for compound **2** at 1400 Oe in the temperature range 2-5.5 K.

| $T$ / K | $\chi_S$ / cm$^3$ mol$^{-1}$ | $\chi_T$ / cm$^3$ mol$^{-1}$ | $\tau$ / s | $\alpha$ | $R^2$ |
|---|---|---|---|---|---|
| 2 | 0.44267 | 0.85998 | 3.8616E-4 | 0.32528 | 0.99987 |
| 2.2 | 0.41012 | 0.80184 | 3.36478E-4 | 0.2961 | 0.99983 |
| 2.4 | 0.38103 | 0.75372 | 2.95939E-4 | 0.28018 | 0.99976 |
| 2.6 | 0.35735 | 0.71094 | 2.62713E-4 | 0.26686 | 0.99974 |
| 2.8 | 0.3397 | 0.67078 | 2.32467E-4 | 0.24406 | 0.99968 |
| 3 | 0.32621 | 0.6341 | 2.06276E-4 | 0.21467 | 0.99964 |
| 3.5 | 0.29652 | 0.55891 | 1.48711E-4 | 0.15057 | 0.99968 |
| 4 | 0.26764 | 0.50005 | 9.71502E-5 | 0.10368 | 0.99978 |
| 4.5 | 0.24361 | 0.45239 | 6.0143E-5 | 0.06404 | 0.99981 |

| | | | | | |
|---|---|---|---|---|---|
| 5 | 0.22193 | 0.41417 | 3.62249E-5 | 0.04173 | 0.99985 |
| 5.5 | 0.20208 | 0.38289 | 2.14462E-5 | 0.03285 | 0.9997 |

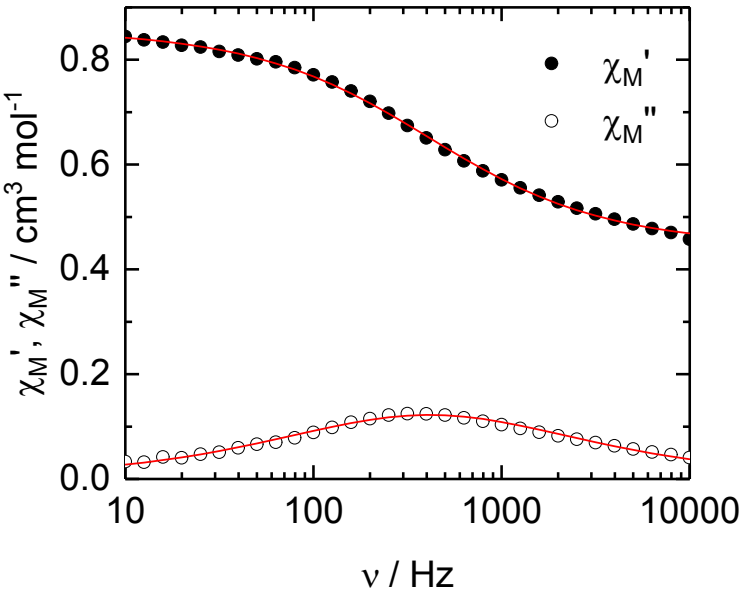


**Figure S9**. Frequency dependence of the in-phase ($\chi_M$') and out-of-phase ($\chi_M$'') components of the AC susceptibility measured on powder at 2 K at 1400 Oe with the best fitted curves (red lines) for **2**.

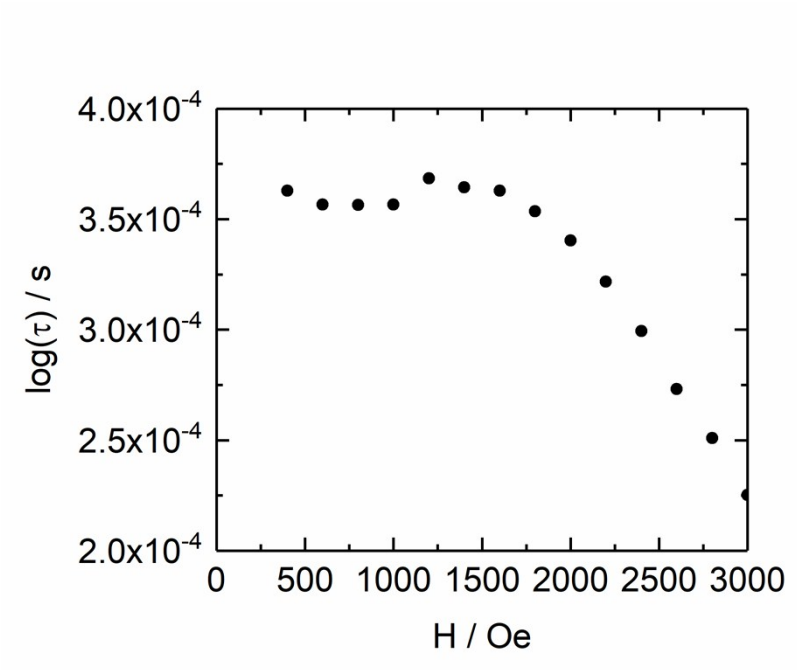


**Figure S10**. Field dependence of the magnetic relaxation time for **2** at 2 K.

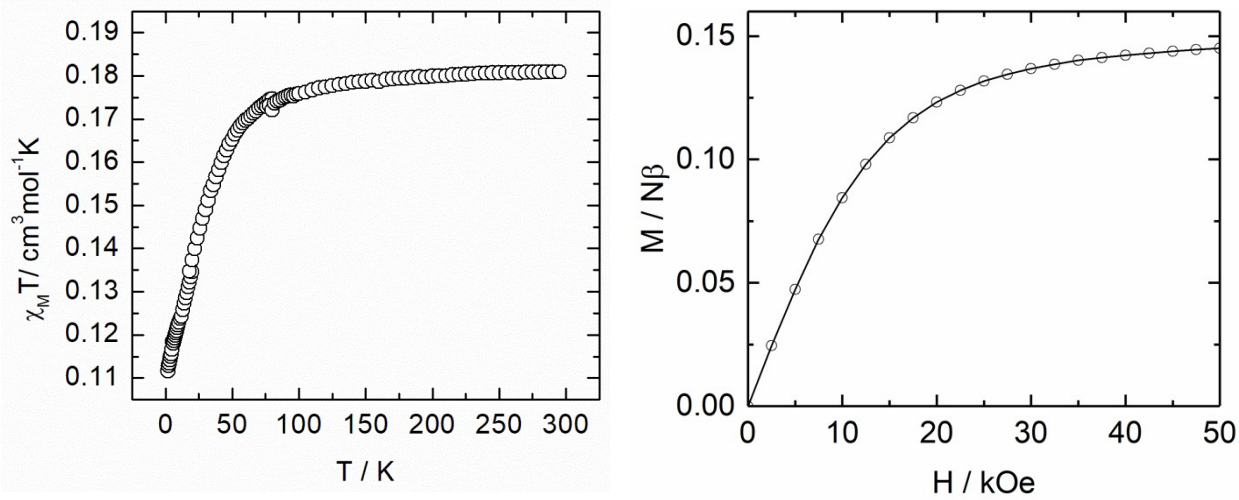


**Figure S11**. Temperature-dependent magnetic susceptibility and magnetization curve at 2 K of $\mathbf{2_{10}}$.

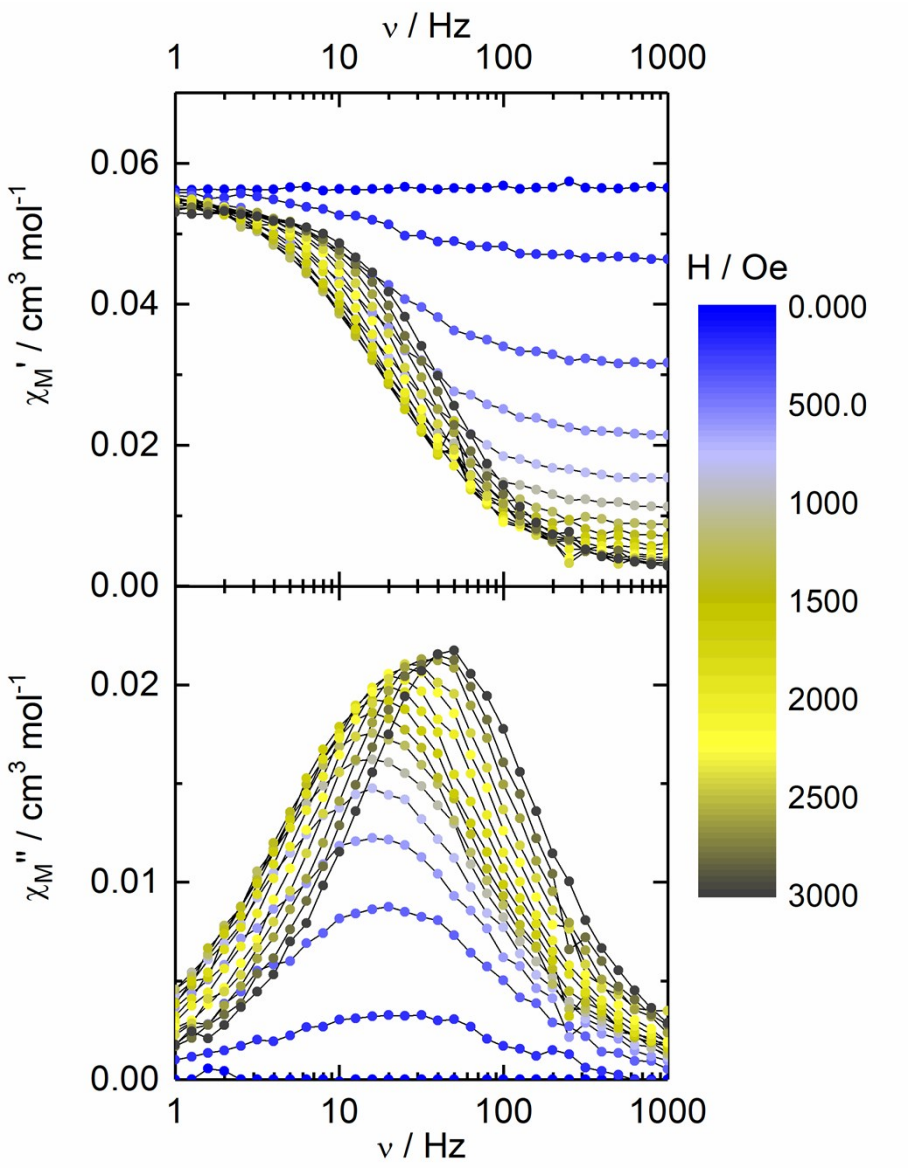


**Figure S12**. Frequency dependences of the in-phase, $\chi_M$', and out-of-phase, $\chi_M$'', components of the AC susceptibility measured at 2 K at various external DC fields for compound $\mathbf{2_{10}}$.

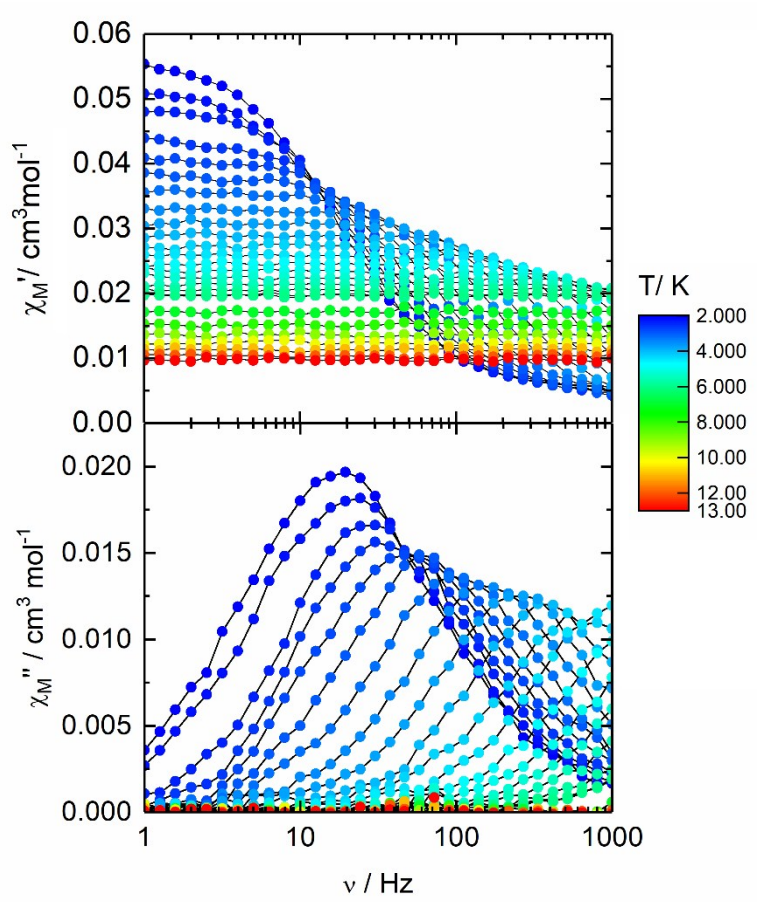


**Figure S13**. Temperature variations of $\chi_M$' and $\chi_M$'' for compound $\mathbf{2_{10}}$ as a function of the frequency, $\nu$ of the oscillating AC field measured at an external DC field of 1600 Oe.

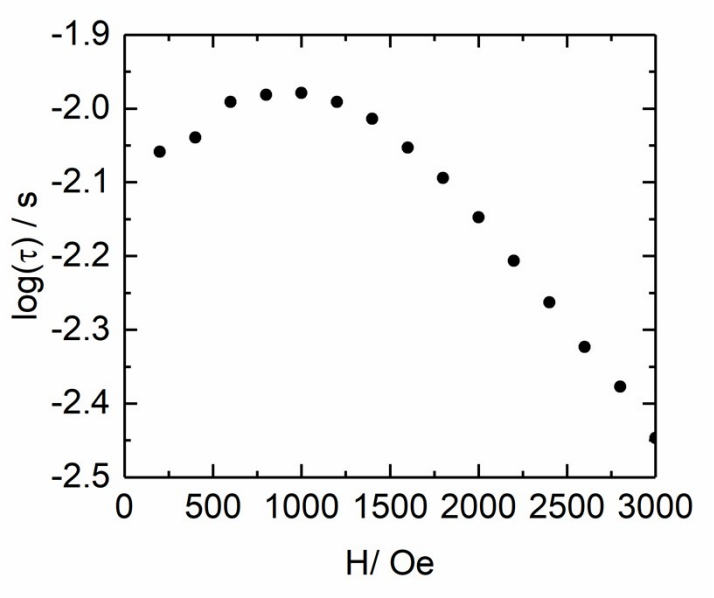


**Figure S14**. Field dependence of the magnetic relaxation time for $\mathbf{2_{10}}$ at 2 K.

**Table S4**. Best fitted parameters ($\chi_T$, $\chi_S$, $\tau$ and $\alpha$) with the extended Debye model for compound $\mathbf{2_{10}}$ at 2 K between 0 and 3000 Oe.

| $H$ / Oe | $\chi_S$ / cm$^3$ mol$^{-1}$ | $\chi_T$ / cm$^3$ mol$^{-1}$ | $\tau$ / s | $\alpha$ | R² |
|---|---|---|---|---|---|
| 0 | NA | 0.05646 (average) | NA | NA | NA |
| 200 | 0.04645 | 0.05614 | 0.00874 | 0.21887 | 0.9999 |
| 400 | 0.03109 | 0.05608 | 0.00914 | 0.21435 | 0.99981 |
| 600 | 0.02096 | 0.05648 | 0.0102 | 0.22033 | 0.99967 |
| 800 | 0.01454 | 0.05645 | 0.01044 | 0.21779 | 0.99982 |
| 1000 | 0.01054 | 0.05668 | 0.01049 | 0.20911 | 0.99976 |
| 1200 | 0.00808 | 0.05672 | 0.01021 | 0.19497 | 0.99945 |
| 1400 | 0.0066 | 0.05677 | 0.00968 | 0.18862 | 0.99916 |
| 1600 | 0.00553 | 0.05647 | 0.00885 | 0.18074 | 0.99611 |
| 1800 | 0.00467 | 0.05629 | 0.00805 | 0.16011 | 0.99923 |
| 2000 | 0.00396 | 0.05554 | 0.00712 | 0.14028 | 0.99977 |
| 2200 | 0.00325 | 0.05524 | 0.00621 | 0.12959 | 0.99947 |
| 2400 | 0.00266 | 0.05495 | 0.00546 | 0.13244 | 0.99935 |
| 2600 | 0.0028 | 0.05454 | 0.00475 | 0.11715 | 0.9998 |
| 2800 | 0.00286 | 0.05389 | 0.00419 | 0.10753 | 0.99958 |

| | | | | | |
|---|---|---|---|---|---|
| 3000 | 0.00233 | 0.05359 | 0.00358 | 0.11021 | 0.99975 |

**Table S5**. Best fitted parameters ($\chi_T$, $\chi_S$, $\tau$ and $\alpha$) with the extended Debye model for compound **$2_{10}$** at 1600 Oe in the temperature range 2-4.25 K.

| T / K | $\chi_S$ / cm$^3$ mol$^{-1}$ | $\chi_T$ / cm$^3$ mol$^{-1}$ | $\tau$ / s | α | $R^2$ |
|---|---|---|---|---|---|
| 2 | 0.0052 | 0.05676 | 0.00903 | 0.16629 | 0.99956 |
| 2.2 | 0.00495 | 0.05221 | 0.00749 | 0.15998 | 0.99963 |
| 2.4 | 0.00496 | 0.04786 | 0.00546 | 0.13026 | 0.99711 |
| 2.6 | 0.0047 | 0.04354 | 0.00416 | 0.11772 | 0.99808 |
| 2.8 | 0.00418 | 0.04087 | 0.00311 | 0.11425 | 0.99816 |
| 3 | 0.00423 | 0.03822 | 0.00224 | 0.09409 | 0.99881 |
| 3.25 | 0.0044 | 0.03568 | 0.00153 | 0.07565 | 0.99962 |
| 3.5 | 0.00407 | 0.033 | 9.64E-04 | 0.05839 | 0.99973 |
| 3.75 | 0.00404 | 0.03088 | 6.37E-04 | 0.02949 | 0.99944 |
| 4 | 0.00428 | 0.02894 | 4.24E-04 | 0.00969 | 0.99947 |
| 4.25 | 0.00347 | 0.02729 | 2.59E-04 | 0.02786 | 0.99949 |

**Table S6**. Literature reports of five coordinated $Co^{II}$ complexes and their Spin Hamiltonian parameters. We can include this Table after we get the SH parameters

| Compound | Geometry | $D$ (cm$^{-1}$) | $E$ (cm$^{-1}$) | $g$ | $U_{eff}$(cm$^{-1}$) | Reference |
|---|---|---|---|---|---|---|
| $[Co(NS_3{}^{iPr})Cl]BPh_4$ | TBPY | -19.1 | 1.5 | 2.43 | 32 | S1 |
| $[Co(NS_3{}^{tBu})Cl]\ ClO_4$ | TBPY | -21.4 | - | 2.29 | | S2 |
| $[Co(NS_3{}^{tBu})Br]\ ClO_4$ | TBPY | -20.2 | - | 2.29 | 21 | |
| $[Co(NS_3{}^{tBu})NCS]\ ClO_4$ | TBPY | -11.0 | - | 2.29 | 20 | |
| $[Co(TPMA)(CH_3CN)](BF_4)_2{\cdot}CH_3CN$ | TBPY | 9.6 | 0.2 | 2.29 | - | S3 |
| $[Co(TPMA)Cl]Cl.2{\cdot}4(H_2O)$ | TBPY | -6.9 | -1.78 | 2.35 | | |
| [Co(TPMA)Cl]Cl | TBPY | -8.4 | 0 | 2.30 | | |
| $[Co(TPMA)Br]Br.2{\cdot}0(H_2O)$ | TBPY | -6.3 | 1.6 | 2.34 | | |
| [Co(TPMA)Br]Br | TBPY | -7.1 | 0 | - | | |

| | | | | | | |
|---|---|---|---|---|---|---|
| [Co(TPMA)I]I | TBPY | -7.5 | 1 | | | |
| $[Co(PP_3)Cl]ClO_4$ | SPY | 46.4 | 10.1 | 2.31 | 37.8 | S4 |
| $[Co(PP_3)Br]ClO_4$ | SPY | 40.7 | 9.3 | 2.28 | 34.5 | |
| $[Co^{II}(NNN^{-pyr})Cl_2]$ | SPY | 150 | 11.6 | $g_z$=2.00; $g_{xy}$= 3.28 | - | S5 |
| $[Co^{II}(NNN^{-ip\text{-}Me})SCN_2]$ | SPY | -28.8 | - | - | 11.1 | S6 |
| $[Co^{II}(NNN^{-ip\text{-}ph})SCN_2]$ | SPY | -28.8 | - | - | 16.7 | |
| $[Co(Me_4cyclam)N_3]^+$ | SPY | 30 | 9.8 | $g_z$= 2.03; $g_{xy}$= 2.35 | 2.3 | S7 |
| $[Co^{II}(NNN^{-bim})Cl]$ | SPY | 14.5 | 0 | $g_x$=2.41; $g_y$=2.25; $g_z$=2.01 | 19.6 | S8 |
| $[Co^{II}(NNN^{-bim})Br]$ | SPY | 8.4 | 0 | $g_x$=2.3; $g_y$=2.2; $g_z$=1.99 | 8.2 | |
| $[Co(tpa)Cl]ClO_4$ | SPY | -10.1 | 1.8 | - | 12 | S9 |
| $[Co(tpa)Br]ClO_4$ | SPY | -7.8 | 2.1 | - | 8.7 | |
| $[Co(tbta)Cl](ClO_4)(MeCN)_2(H_2O)$ | SPY | -7.5 | 0.4 | - | 8.1 | |
| $[Co(tbta)Br]ClO_4$ | SPY | -4.3 | 0.03 | - | 5 | |
| $[Co(N_3)LH_3]^{4+}$ | SPY | -7.1 | - | $g_z$= 2.24; $g_{xy}$= 2.36 | 14.2 | S10 |
| $[Co(terpy)Cl_2]$ | SPY | - | - | $g_x$=1.35; $g_y$=1.93; $g_z$=7.75 | 19.5<br>2.8 | S11 |
| $[Co(terpy)(NCS)_2]$ | SPY | - | - | - | 11.8<br>2.1 | |
| $[Co(bzimpy)Cl_2]$ | SPY | 71.7 | 1.4 | $g_x$=2.5; $g_y$=2.62; $g_z$=1.47 | - | S12 |
| $[CoL^1Cl_2]$ | SPY | 71.7 | 0 | $g_z$= 2.0; $g_{xy}$= 2.5 | - | S13 |
| $[CoL^2Cl_2]$ | SPY | 46.8 | 0 | $g_z$= 2.0; $g_{xy}$= 2.35 | - | |
| $[Co(L)Cl_2]\cdot CH_3OH]$ | TBPY | | | | | This work |
| [Co(L)Br2] | SPY | | | | | |
| [Co(L)(NCS)2] | TBPY | | | | | |

$Me_6$tren: hexamethyltris(aminoethyl)amine; $NS_3^{iPr}$: tris-(2-(isopropylthio)ethyl)amine; $NS_3^{tBu}$: tris-(2-(tertbutyl)thio)ethyl)amine; $Me_4$cyclam: tetramethylcyclam, $N_3$: azido; $PP_3$: tris[2-(diphenylphosphino)ethyl]-phosphine; $NNN^{-pyr}$: 4-hept-1-ynyl-2,6-dipyrazol-1-

ylpyridine; ($NNN^{-ip}$) : bis(imino)pyridine; terpy: terpyridine; bzimpy: 2,6-bis(benzimidazol-2-yl)pyridine; $L^1$: 4'-iodo-2',6'-dipyrazolyl-pyridine; $L^2$: 4′-dodecynyl-2′,6′-dipyrazolyl pyridine; $LH_3$:6,16,2,5-tribenzena(1,4)-1,4,8,11,14,18,23,27-octaazabicyclo[9.9.9]nonacosaphane; TBP: Trigonal Bipyramid; SqPy: Square Pyramid

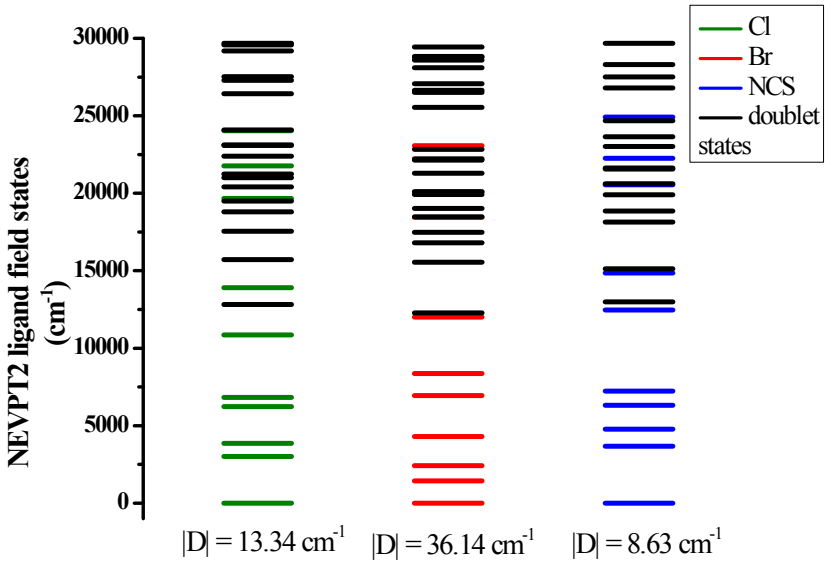


**Figure S15**. NEVPT2 transition energies of quartet and doublet states (up to 30000 $cm^{-1}$ shown) of the three complexes.

**Table S7** . NEVPT2 transition energies, their corresponding wavefunction and their individual contributions towards D and E value for the ground state and 1st four excited states for complex **1**.

| Spin free energy states of Complex **1** | Major CASSCF electronic configuration | NEVPT2 transition energy ($cm^{-1}$) | Contribution to D ($cm^{-1}$) | Contribution to E ($cm^{-1}$) |
|---|---|---|---|---|
| GS | $d_{xz}^2 d_{xy}^2 d_{yz}^1 d_{z^2}^1 d_{x^2-y^2}^1$(51%) | 0.0 | 0.0 | 0.0 |

| | | | | |
|---|---|---|---|---|
| | $d_{xz}^1d_{xy}^2d_{yz}^1\ d_{z^2}^2\ d_{x^2-y^2}^1$(24%)<br>$d_{xz}^2d_{xy}^1d_{yz}^1\ d_{z^2}^2\ d_{x^2-y^2}^1$(16%) | | | |
| 1st ES | $d_{xz}^1d_{xy}^2d_{yz}^2\ d_{z^2}^1\ d_{x^2-y^2}^1$(35%)<br>$d_{xz}^1d_{xy}^2d_{yz}^1\ d_{z^2}^2\ d_{x^2-y^2}^1$(27%)<br>$d_{xz}^2d_{xy}^2d_{yz}^1\ d_{z^2}^1\ d_{x^2-y^2}^1$(14%) | 3017.3 | 14.2 | 12.2 |
| 2nd ES | $d_{xz}^2d_{xy}^1d_{yz}^2\ d_{z^2}^1\ d_{x^2-y^2}^1$(71%) | 3858.1 | 9.7 | -9.0 |
| 3rd ES | $d_{xz}^1d_{xy}^2d_{yz}^2\ d_{z^2}^1\ d_{x^2-y^2}^1$(42%)<br>$d_{xz}^1d_{xy}^2d_{yz}^1\ d_{z^2}^2\ d_{x^2-y^2}^1$(35%) | 6236.3 | 1.0 | 0.0 |
| 4th ES | $d_{xz}^2d_{xy}^1d_{yz}^1\ d_{z^2}^1\ d_{x^2-y^2}^2$(40%)<br>$d_{xz}^1d_{xy}^1d_{yz}^1\ d_{z^2}^2\ d_{x^2-y^2}^2$(19%) | 6823.1 | -12.1 | -0.4 |

**Table S8**. NEVPT2 transition energies, their corresponding wavefunction and their individual contributions towards D and E value for the ground state and 1st five excited states for complex **2**.

| Spin free energy states of Complex **2** | Major CASSCF electronic configuration | NEVPT2 transition energy ($cm^{-1}$) | Contribution to D ($cm^{-1}$) | Contribution to E ($cm^{-1}$) |
|---|---|---|---|---|
| GS | $d_{xy}^2\ d_{z^2}^2d_{yz}^1d_{xz}^1\ d_{x^2-y^2}^1$(57%)<br>$d_{xy}^1\ d_{z^2}^2d_{yz}^1d_{xz}^1\ d_{x^2-y^2}^2$(19%) | 0.0 | 0.0 | 0.0 |
| 1st ES | $d_{xy}^2\ d_{z^2}^1d_{yz}^2d_{xz}^1\ d_{x^2-y^2}^1$(45%)<br>$d_{xy}^1d_{z^2}^2d_{yz}^1d_{xz}^2\ d_{x^2-y^2}^1$(15%) | 1439.4 | 22.7 | -20.2 |
| 2nd ES | $d_{xy}^1\ d_{z^2}^2d_{yz}^2d_{xz}^1\ d_{x^2-y^2}^1$(22%)<br>$d_{xy}^2\ d_{z^2}^1d_{yz}^2d_{xz}^1\ d_{x^2-y^2}^1$(18%)<br>$d_{xy}^1\ d_{z^2}^1d_{yz}^2d_{xz}^2\ d_{x^2-y^2}^1$(16%) | 2423.4 | 29.2 | 27.4 |
| 3rd ES | $d_{xy}^1\ d_{z^2}^1d_{yz}^2d_{xz}^2\ d_{x^2-y^2}^1$(48%)<br>$d_{xy}^2\ d_{z^2}^1d_{yz}^1d_{xz}^2\ d_{x^2-y^2}^1$(20%) | 4297.3 | 0.2 | 0.2 |
| 4th ES | $d_{xy}^1\ d_{z^2}^1d_{yz}^2d_{xz}^1\ d_{x^2-y^2}^2$(35%)<br>$d_{xy}^1\ d_{z^2}^1d_{yz}^2d_{xz}^2\ d_{x^2-y^2}^1$(21%) | 6947.5 | 0.5 | 0.5 |
| 5th ES | $d_{xy}^1\ d_{z^2}^2d_{yz}^1d_{xz}^1\ d_{x^2-y^2}^2$(51%)<br>$d_{xy}^2\ d_{z^2}^2d_{yz}^1d_{xz}^1\ d_{x^2-y^2}^1$(17%) | 8363.7 | -11.9 | -0.1 |

**Table S9**. NEVPT2 transition energies, their corresponding wave function and their individual contributions towards D and E value for the ground state and 1st four excited states for complex **3**.

| Spin free energy states of Complex **3** | Major CASSCF electronic configuration | NEVPT2 transition energy ($cm^{-1}$) | Contribution to D ($cm^{-1}$) | Contribution to E ($cm^{-1}$) |
|---|---|---|---|---|

| | | | | |
|---|---|---|---|---|
| GS | $d_{xy}^2d_{xz}^2d_{yz}^1\ d_{x^2-y^2}^1\ d_{z^2}^1$(31%)<br>$d_{xy}^2d_{xz}^1d_{yz}^1\ d_{x^2-y^2}^1\ d_{z^2}^2$(22%) | 0.0 | 0.0 | 0.0 |
| 1st ES | $d_{xy}^1d_{xz}^2d_{yz}^2\ d_{x^2-y^2}^1\ d_{z^2}^1$(42%)<br>$d_{xy}^1d_{xz}^1d_{yz}^1\ d_{x^2-y^2}^2\ d_{z^2}^2$(18%) | 3674.9 | -0.3 | -7.8 |
| 2nd ES | $d_{xy}^1d_{xz}^1d_{yz}^2\ d_{x^2-y^2}^2\ d_{z^2}^1$(47%)<br>$d_{xy}^2d_{xz}^1d_{yz}^2\ d_{x^2-y^2}^1\ d_{z^2}^1$(31%) | 4781.4 | -9.3 | -2.7 |
| 3rd ES | $d_{xy}^1d_{xz}^1d_{yz}^1\ d_{x^2-y^2}^2\ d_{z^2}^2$(22%)<br>$d_{xy}^1d_{xz}^2d_{yz}^1\ d_{x^2-y^2}^2\ d_{z^2}^1$(19%)<br>$d_{xy}^1d_{xz}^2d_{yz}^1\ d_{x^2-y^2}^1\ d_{z^2}^2$(17%) | 6316.9 | -5.1 | -0.3 |
| 4th ES | $d_{xy}^2d_{xz}^1d_{yz}^1\ d_{x^2-y^2}^1\ d_{z^2}^2$(28%)<br>$d_{xy}^1d_{xz}^2d_{yz}^1\ d_{x^2-y^2}^2\ d_{z^2}^1$(21%)<br>$d_{xy}^1d_{xz}^1d_{yz}^1\ d_{x^2-y^2}^2\ d_{z^2}^2$(19%) | 7229.2 | 7.6 | 7.5 |

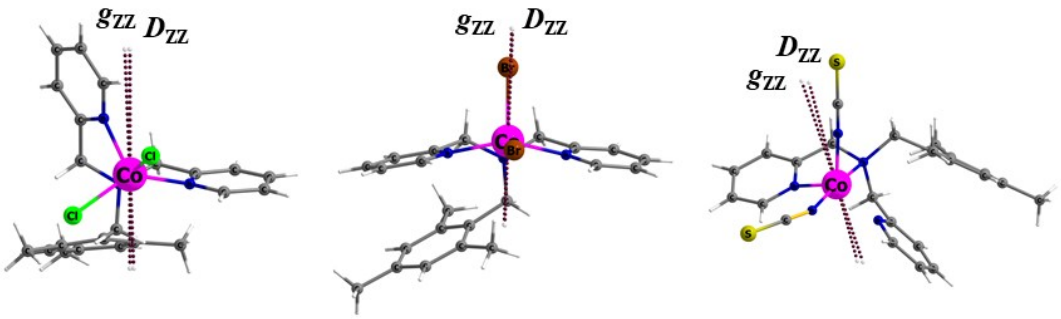


**Figure S16**. Z-component of the *D* and *g*-anisotropy axes ($g_{zz}$ and $D_{zz}$) of the three complexes **1-3** respectively.

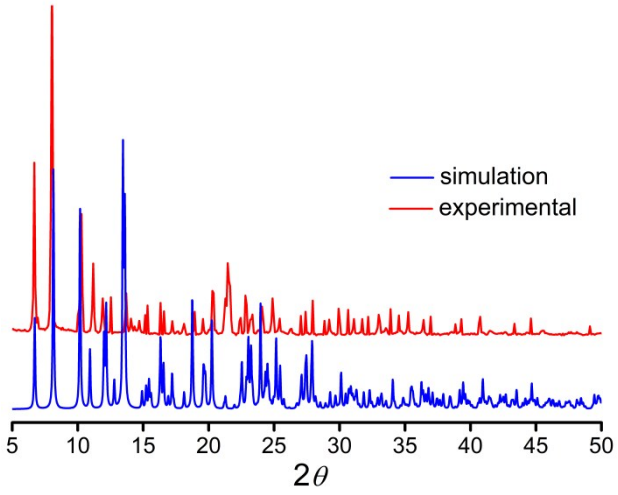


**Figure S17**. Experimental and simulated PXRD pattern for complex **1**.

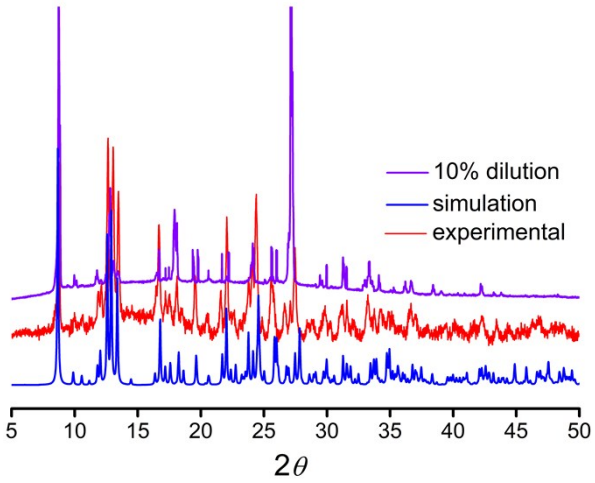


**Figure S18**. Experimental and simulated PXRD pattern for complex **2** and 10% diluted sample, $\mathbf{2_{10}}$.

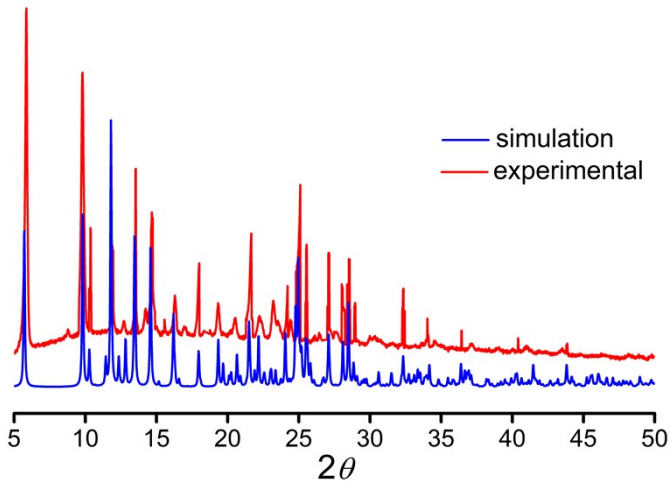


**Figure S19**. Experimental and simulated PXRD pattern for complex **3.**

**References**

S1. F. Shao, B. Cahier, N. Guihéry, E. Rivière, R. Guillot, A.-L. Barra, Y. Lan, W. Wernsdorfer, V. E. Campbell and T. Mallah, *Chem. Commun.*, 2015, **51**, 16475-16478.

S2. F. Shao, B. Cahier, E. Rivière, R. Guillot, N. Guihéry, V. E. Campbell and T. Mallah, *Inorg. Chem.*, 2017, **56**, 1104-1111.

S3. T. J. Woods, M. F. Ballesteros-Rivas, S. Gómez-Coca, E. Ruiz and K. R. Dunbar, *J. Am. Chem. Soc.*, 2016, **138**, 16407-16416.

S4. A. K. Mondal, J. Jover, E. Ruiz and S. Konar, *Chem. Commun.*, 2017, **53**, 5338-5341.

S5. C. Rajnák, J. Titiš, O. Fuhr, M. Ruben and R. Boča, *Inorg. Chem.*, 2014, **53**, 8200-8202.

S6. T. Jurca, A. Farghal, P.-H. Lin, I. Korobkov, M. Murugesu and D. S. Richeson, *J. Am. Chem. Soc.*, 2011, **133**, 15814-15817.

S7. B. Cahier, M. Perfetti, G. Zakhia, D. Naoufal, F. El-Khatib, R. Guillot, E. Rivière, R. Sessoli, A.-L. Barra, N. Guihéry and T. Mallah, *Chem.-Eur. J.*, 2017, **23**, 3648-3657.

S8. A. K. Mondal, T. Goswami, A. Misra and S. Konar, *Inorg. Chem.*, 2017, **56**, 6870-6878.

S9. A. K. Mondal, J. Jover, E. Ruiz and S. Konar, *Chem.-Eur. J.*, 2017, **23**, 12550-12558.

S10. F. El-Khatib, B. Cahier, F. Shao, M. López-Jordà, R. Guillot, E. Rivière, H. Hafez, Z. Saad, J.-J. Girerd, N. Guihéry and T. Mallah, *Inorg. Chem.*, 2017, **56**, 4601-4608.

S11. F. Habib, O. R. Luca, V. Vieru, M. Shiddiq, I. Korobkov, S. I. Gorelsky, M. K. Takase, L. F. Chibotaru, S. Hill, R. H. Crabtree and M. Murugesu, *Angew. Chem. Int. Ed.*, 2013, **52**, 11290-11293.

S12. R. Boča, L. u. Dlháň, W. Linert, H. Ehrenberg, H. Fuess and W. Haase, *Chem. Phys. Lett.*, 1999, **307**, 359-366.

S13. C. Rajnák, J. Titiš, I. Šalitroš, R. Boča, O. Fuhr and M. Ruben, *Polyhedron*, 2013, **65**, 122-128.